

Harnessing Increased Client Participation with Cohort-Parallel Federated Learning

Akash Dhasade,¹ Anne-Marie Kermarrec,¹ Tuan-Anh Nguyen,² Rafael Pires,¹ Martijn de Vos¹

¹ EPFL

² University Grenoble Alpes

Abstract

Federated learning (FL) is a machine learning approach where nodes collaboratively train a global model. As more nodes participate in a round of FL, the effectiveness of individual model updates by nodes also diminishes. In this study, we increase the effectiveness of client updates by dividing the network into smaller partitions, or *cohorts*. We introduce Cohort-Parallel Federated Learning (CPFL): a novel learning approach where each cohort independently trains a global model using FL, until convergence, and the produced models by each cohort are then unified using one-shot knowledge distillation (KD) and a cross-domain, unlabeled dataset. The insight behind CPFL is that smaller, isolated networks converge quicker than in a one-network setting where all nodes participate. Through exhaustive experiments involving realistic traces and non-IID data distributions on the CIFAR-10 and FEMNIST image classification tasks, we investigate the balance between the number of cohorts, model accuracy, training time, and compute and communication resources. Compared to traditional FL, CPFL with four cohorts, non-IID data distribution, and CIFAR-10 yields a $1.9\times$ reduction in train time and a $1.3\times$ reduction in resource usage, with a minimal drop in test accuracy.

1 Introduction

Federated learning (FL) allows for the collaborative training of a machine learning model across a distributed network of training nodes, or clients, without ever moving training data (McMahan et al. 2017). A central server orchestrates the process by selecting a subset of clients, referred to as a *cohort*, and sends them the most recent version of the global model. Subsequently, clients in this cohort undertake a few training steps on their local datasets, contributing to the refinement of the model. The locally updated models are then transmitted back to the server for aggregation. This iterative process continues with the server selecting another cohort, possibly composed of a different set of clients, for each successive training round until the global model converges.

The effect of the cohort size on FL performance has been assessed in numerous studies (McMahan et al. 2017; Charles et al. 2021; Huba et al. 2022). While larger cohort sizes intuitively learn from more data in each round, thus accelerating the convergence of the global model, they have been found to yield diminishing returns (Charles et al. 2021). Furthermore, larger cohorts often use client updates inefficiently,

requiring more resources and time to reach similar accuracy levels compared to smaller cohort sizes (Charles et al. 2021; Huba et al. 2022). As a result, current methods struggle to fully take advantage of model updates from a large number of clients (Bonawitz et al. 2019).

This work explores a strategy that harnesses increased client participation more efficiently. FL research traditionally focuses on the one-cohort setting and speeds up model convergence by increasing the size of a cohort (Bonawitz et al. 2019). We instead propose and investigate the simple idea of *partitioning* the network into several cohorts¹, each of which runs independent and parallel FL training sessions. We name this approach *Cohort-Parallel Federated Learning*, or CPFL. The architecture of CPFL is illustrated in Figure 1. Clients within a cohort contribute to training a model specific to that cohort (step 1). This cohort model is trained until convergence and uploaded to a single FL server (step 2). Finally, the server unifies these multiple cohort models into a single global model through the process of Knowledge distillation (KD) (step 3). KD is a technique that combines the knowledge of different teacher models into a unified student model (Hinton, Vinyals, and Dean 2015). We leverage cross-domain, unlabeled and public datasets to carry out KD and produce the final model.

CPFL provides three main benefits compared to single-cohort FL. Firstly, smaller networks make more efficient use of client updates, reducing the computation and communication resources required to train a model. Secondly, smaller networks converge significantly quicker than the entire network, reducing overall training time. We illustrate this effect in Figure 2, which shows the evolution of validation loss without partitioning the network (dashed curve) and when partitioning the network (solid curves). We annotate with vertical lines the round when models have converged, according to our stopping criterion described in Section 4.1. From this figure, it is evident that smaller partitions converge faster than when the network is not partitioned, both with IID and non-IID data distributions. Thirdly, partitioning the network into smaller cohorts provides a flexible means to control resource usage and time to convergence by appropriately choosing number of cohorts. Our proposal is generic and can therefore be applied to any FL setting.

¹We refer to network partitions as *cohorts* throughout this work.

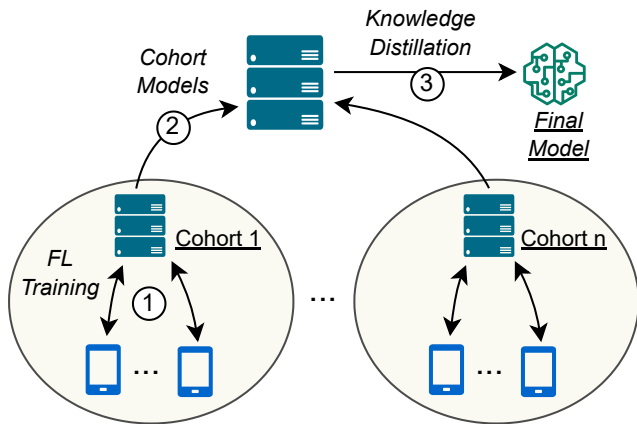


Figure 1: The architecture of Cohort-Parallel Federated Learning (CPFL).

Contributions.

- We propose CPFL, which uses partitioning as a simple and effective strategy to improve FL performance.
- We provide theoretical guarantees on the performance of the global model through domain adaptation analysis. Our result extends KD to a more general setting where the teacher model is composed of a mixture of distributions, as is the case for CPFL.
- We conduct extensive experiments using realistic traces of devices exhibiting different compute and network speeds on two image classification datasets with varying data distributions. We analyze the effect of the number of cohorts in CPFL on the achieved test accuracy, resource utilization, and training time. Our results on the CIFAR-10 dataset under non-IID data distributions demonstrate that employing just four cohorts can already lead to a $1.3\times$ reduction in training resource usage and $1.9\times$ faster convergence with a minimal drop in test accuracy of 0.6% compared to traditional FL.

In summary, CPFL offers FL practitioners a simple and pragmatic method to obtain considerable resource savings and shorter training sessions in FL systems.

2 Related Work

Cohorts in Federated Learning. The idea of grouping clients *under some criterion* referred to as *clustering* has been well-studied in the FL literature (Ghosh et al. 2020; Duan et al. 2021; Liu et al. 2022). The first set of these works leverages clustering to solve the federated multi-task learning (FMTL) problem, which assumes that there exist k different data distributions $\mathcal{D}_1, \mathcal{D}_2, \dots, \mathcal{D}_K$ in a network of m clients. Each distribution \mathcal{D}_i corresponds to a different task i where these approaches aim to cluster clients that solve similar tasks without the explicit knowledge of cluster identities (Ghosh et al. 2020; Sattler, Müller, and Samek 2020). The second set of works focuses on mitigating the impact of data non independent and identically distributed (non-IID)ness or client data distribution shift (*e.g.*, concept

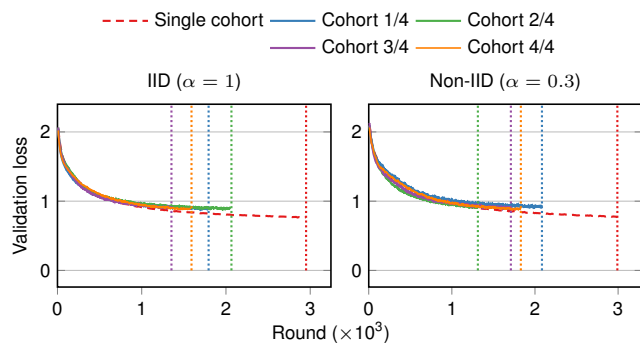


Figure 2: Comparison of validation loss for both partitioned (solid curves) and unpartitioned (dashed curve) networks across IID (left figure) and non-IID (right figure) distributions. The vertical dotted line denotes the convergence point of the training. Additional details are provided in Appendix B.2.

shift) by clustering statistically similar clients (Briggs, Fan, and Andras 2020; Liu et al. 2022). Such clustering relies on some statistics collected during training *e.g.*, similarity of gradient or model updates obtained from clients, and typically introduces overheads to obtain clusters. In contrast to the above works, we study and showcase the benefits of *partitioning i.e.*, simply dividing the network into arbitrary groups of clients. Uniquely, our work explores the trade-offs between time to convergence, resource usage, and attained accuracies intricately tied to the number of partitions.

Parallelism in Federated Learning. The parallelism induced by increasing the number of participating clients per round was initially investigated by McMahan *et al.* (2017). They observed that leveraging more clients per round reduced the number of rounds required to reach a target accuracy. However, the benefits extended only to a certain threshold number of clients, beyond which the returns diminished significantly. Charles *et al.* (2021) further examined the impact of large client participation across various learning tasks. The conclusions were similar, where the threshold was empirically shown to lie between 10 and 50, interestingly the same for all tasks. In a network of thousands of clients with several hundred available clients per round, this empirical threshold clearly illustrates the limitations of current methods in effectively utilizing increased client participation. (Charles et al. 2021) also show that federated algorithms under large client participation use local updates inefficiently, requiring significantly more samples per unit-accuracy. These limitations call for a novel approach that can better capitalize increased parallelism (Bonawitz et al. 2019).

Knowledge Distillation (KD). In this work, we leverage KD to combine the knowledge of individual cohort models into a single global model at the server. KD was initially proposed to extract information from a complex teacher model into a small student model (Hinton, Vinyals, and Dean 2015). Conventionally, the training of the student model in-

Algorithm 1: Cohort-Parallel Federated Learning

Input: Set of n cohorts $\{\mathcal{C}_i\}_{i=1}^n$, aggregation weights $\{p_i\}_{i=1}^n$, learning rate η , public dataset $\hat{\mathcal{D}}_p$, parametric function f from h_θ , number of epochs E

Output: Final global model parameters θ

Cohort Servers Execute

for each cohort $i = 1, \dots, n$ *in parallel* **do**

$\theta_i \leftarrow$ train model using standard FL
 Send θ_i to the global server

end

Global Server Executes

Initialize global model parameters θ_s

for $x \in \hat{\mathcal{D}}_p$ **do**

for $i = 1, \dots, n$ **do**

$z_i \leftarrow f(x; \theta_i)$

end

$\tilde{z} \leftarrow \sum_{i=1}^n p_i z_i$ \triangleright aggregate

end

for $e = 1, \dots, E$ **do**

for mini-batch $b \in \hat{\mathcal{D}}_p$ **do**

$z_s \leftarrow f(b; \theta_s)$

$\theta_s \leftarrow \theta_s - \eta \cdot \nabla_{\theta_s} \mathcal{L}$ \triangleright eq. (3)

end

end

return θ

volves the minimization of the disparity between the logits produced by the student and teacher, which are computed utilizing an appropriate auxiliary dataset (Hinton, Vinyals, and Dean 2015). KD has been increasingly used in FL to reduce communication costs (He, Annavaram, and Avestimehr 2020; Sattler et al. 2022; Gong et al. 2022), enable heterogeneous client models (Li and Wang 2019; Lin et al. 2020) or mitigate privacy risks (Gong et al. 2022). More generally, KD has also been used to exchange knowledge in a distributed network of clients (Bistriz, Mann, and Bambos 2020; Zhmoginov et al. 2023).

We highlight two algorithms in the literature that are special cases of our proposed CPFL algorithm. One extreme is the one-shot FedKD algorithm (Gong et al. 2022) wherein each node or client is its own cohort. On the other extreme is the standard FedAvg algorithm (McMahan et al. 2017) where all nodes belong to a single cohort. In particular, FedAvg does not utilize KD since there is only one cohort, requiring no knowledge fusion. CPFL can proficiently navigate this spectrum, exhibiting interesting characteristics that can be controlled by altering the number of cohorts.

3 Cohort-Parallel Federated Learning

We now describe CPFL, a learning approach that combines the strength of multiple parallel FL sessions with KD. We illustrate our approach in Figure 1 and provide pseudocode in Algorithm 1.

3.1 Algorithm Overview

Consider a supervised learning problem with input space \mathcal{X} and output space \mathcal{Y} . We define a finite hypothesis class parameterized by $\Theta \subset \mathbb{R}^d$ as $\mathcal{H} = \{h_\theta, \theta \in \Theta\}$. We use h_θ to designate a hypothesis and θ to represent the model parameters, unless stated otherwise. Let $h_\theta = g \circ f$, where $f: \mathcal{X} \rightarrow \mathbb{R}^{|\mathcal{Y}|}$ refers to a parametric function that produces logits to which the prediction function $g: \mathbb{R}^{|\mathcal{Y}|} \rightarrow \mathcal{Y}$ is applied. For instance, in the common case of neural networks, f corresponds to the model until the last layer, and g corresponds to the softmax operation. Given ℓ a non-negative convex loss function, the expected risk of hypothesis h_θ on data distribution \mathcal{D} is defined as $\mathcal{L}_{\mathcal{D}}(\theta) = \mathbb{E}_{(x,y) \sim \mathcal{D}} [\ell(h_\theta(x), y)]$. We consider an FL setting with $M = n * K$ clients², each possessing a local private labeled dataset following distribution $\mathcal{D}_{i,k}$ in $\mathcal{X} \times \mathcal{Y}$.

In the first stage of the algorithm, the global server randomly partitions the clients into n cohorts, each comprising K clients. We opt for a random partitioning of nodes into cohorts due to its simplicity and universality. This approach ensures unbiased division without introducing added complexities or biases that more advanced partitioning strategies might incur³. Each cohort runs parallel and independent FL training sessions using any traditional FL algorithm, e.g., FedAvg, while reporting to its cohort server (step 1 in Figure 1). These servers could, for example, correspond to geographically distributed FL servers running FL sessions within their geographic boundaries or correspond to co-located servers within the single global server. Each such server trains cohort specific parameters θ_i , which minimize the average risk across all clients within a cohort. Precisely, for every $i \in [n]$,

$$\theta_i \in \arg \min_{\theta} \frac{1}{K} \sum_{k=1}^K \mathcal{L}_{\mathcal{D}_{i,k}}(\theta). \quad (1)$$

Each cohort server sends θ_i to the global server after it has converged (step 2 in Figure 1).

In the second stage of the algorithm, the global server distills the knowledge of each cohort model (called teacher models) into a single global model (called the student model) once all cohorts have converged (step 3 in Figure 1). This knowledge transfer is facilitated by an unlabeled public dataset $\hat{\mathcal{D}}_p$. Specifically, the global server generates logit vectors $z_i = f(x; \theta_i)$ for every $x \in \hat{\mathcal{D}}_p$ for each cohort $i \in [n]$. These logits are then aggregated $\tilde{z} := \sum_{i=1}^n p_i z_i$ where p_i denotes the weights of the aggregation with $\sum_{i=1}^n p_i = 1$ to act as soft-targets for the process of knowledge distillation. Denoting by θ_s the parameters of the global server’s model and $z_s = f(x; \theta_s)$, the global server solves the following optimization problem:

$$\theta_s \in \arg \min_{\theta} \mathbb{E}_{x \sim \mathcal{D}_p} [\mathcal{L}(z_s, \tilde{z})] \quad (2)$$

$$\text{where } \mathcal{L}(z_s, \tilde{z}) = \|z_s - \tilde{z}\|_1 \quad (3)$$

²This is for simplicity - our setting still holds otherwise.

³An advanced partitioning scheme could be a multi-objective function that considers data skewness, device characteristics, etc.

and $\|\cdot\|_1$ represents the L1 norm. Our complete approach is outlined in Algorithm 1.

We set the weights for logit aggregation by extending the approach used in one-shot FedKD (Gong et al. 2022) based on the label distribution of clients. Specifically, each cohort server aggregates the label distribution information of each node within the cohort, resulting in the cohort’s label distribution. The global server then assigns per cohort weight based on its aggregated label distribution. Compared to unweighted averaging, this significantly boosts the effectiveness of knowledge distillation since particular cohorts might be better suited to predict particular target classes. However, having individual nodes in a cohort sharing this information might pose a privacy risk. To mitigate this risk, one might consider using privacy-preserving ensembles, e.g., as in one-shot FedKD, where locally computed logits are perturbed using quantization and noise (Gong et al. 2022). Alternatively, one can compute aggregated label distributions using secure hardware (Dhasade et al. 2022), avoiding the leakage of individual label distributions.

3.2 Cross-domain Analysis

In line with our setting, we established a bridge between knowledge distillation and the theory of domain adaptation. The concept of domain adaptation revolves around training a classifier to perform effectively in a target domain using a model previously trained in a source domain. This concept mirrors the structure of our framework, where we distill knowledge from models trained in parallel using FL on multiple distinct distributions within a cohort and subsequently transfer it to a global model. By viewing our framework through this lens, we developed a generalization bound for our distilled model by drawing upon the principles of domain adaptation theory (Ben-David et al. 2010).

Let \mathcal{D} represent the target distribution and \mathcal{H} be the hypothesis class defined in the previous section. With a slight change in notation, we use h in place of h_θ for simplicity and indicate by $\mathcal{L}_{\mathcal{D}}(h)$ the risk of $h \in \mathcal{H}$. We define the $\mathcal{H}\Delta\mathcal{H}$ -divergence between a source distribution \mathcal{D}' and the target distribution \mathcal{D} , $d_{\mathcal{H}\Delta\mathcal{H}}(\mathcal{D}', \mathcal{D})$ as

$$2 \sup_{h, h' \in \mathcal{H}} \left| \mathbb{P}_{\mathbf{x} \sim \mathcal{D}'}(h(\mathbf{x}) \neq h'(\mathbf{x})) - \mathbb{P}_{\mathbf{x} \sim \mathcal{D}}(h(\mathbf{x}) \neq h'(\mathbf{x})) \right|$$

with $\mathcal{H}\Delta\mathcal{H}$ representing the symmetric difference space defined as $\mathcal{H}\Delta\mathcal{H} := \{h(\mathbf{x}) \oplus h'(\mathbf{x}) | h, h' \in \mathcal{H}\}$. Furthermore, we define $\lambda := \inf_{h \in \mathcal{H}} \{\mathcal{L}_{\mathcal{D}'}(h) + \mathcal{L}_{\mathcal{D}}(h)\}$ as the risk for the optimal hypothesis across the two distributions.

For each cohort $i \in [n]$, we designate h_i and \mathcal{D}_i as the respective hypothesis and distribution. Given that each cohort conducts federated training in parallel, we characterize the distribution \mathcal{D}_i as a mixture of distributions from its K clients i.e., $\mathcal{D}_i = \frac{1}{K} \sum_{k=1}^K \mathcal{D}_{i,k}$. Consequently, we consider a problem of $n * K$ sources domain adaptation. Denoting the hypothesis on the global server by $h_s = \sum_{i=1}^n p_i h_i$, we state the following theorem:

Theorem 1. *Let \mathcal{H} be a finite hypothesis class and $h_s := \sum_{i=1}^n p_i h_i$, where $p_i > 0$ and $\sum_{i=1}^n p_i = 1$. Suppose that each source dataset has m instances. Then, for any*

$\delta \in (0, 1)$, with probability at least $1 - \delta$, the expected risk of h_s on the target distribution \mathcal{D} is bounded by:

$$\begin{aligned} \mathcal{L}_{\mathcal{D}}(h_s) &\leq \sum_{i=1}^n \sum_{k=1}^K \frac{p_i}{K} \mathcal{L}_{\hat{\mathcal{D}}_{i,k}}(h_i) \\ &+ \sum_{i=1}^n \sum_{k=1}^K \frac{p_i}{2K} \left(\frac{1}{2} d_{\mathcal{H}\Delta\mathcal{H}}(\mathcal{D}_{i,k}, \mathcal{D}) + \lambda_{i,k} \right) \\ &+ \sqrt{\frac{\log(2nK/\delta)}{2m}} \end{aligned} \quad (4)$$

where $\lambda_{i,k} := \inf_{h \in \mathcal{H}} \{\mathcal{L}_{\mathcal{D}_{i,k}}(h) + \mathcal{L}_{\mathcal{D}}(h)\}$ and $\hat{\mathcal{D}}_{i,k}$ is the observable dataset of the distribution $\mathcal{D}_{i,k}$.

We provide a proof in Appendix A.1. In essence, the theorem states that the loss of the global student model is upper bounded by the weighted average of: i) the risk of each teacher’s model on its client’s data; ii) the discrepancy between the cohort’s client distribution and the target distribution, quantified by the second term on the RHS; and iii) a constant term contingent on the number of data points and the number of sources. Our theorem extends previous works (Lin et al. 2020; Gong et al. 2022) to a more general setting where we distill knowledge from teacher models which themselves are trained on a mixture of their respective client’s distribution.

4 Evaluation

We implement CPFL and explore different trade-offs between achieved accuracy, training time, and resource usage for different data distributions and number of cohorts.

4.1 Experiment Setup

We have implemented CPFL using PyTorch and published all code online (*link omitted due to double-blind review*).

Dataset. We experiment with both the CIFAR-10 and FEMNIST datasets. CIFAR-10 is a common and well-known baseline in machine learning and consists of 50 000 color images, divided amongst ten classes (Krizhevsky, Hinton et al. 2009). FEMNIST contains 805 263 grayscale images, divided amongst 62 classes (Caldas et al. 2019). As backbone models, we use a LeNet architecture (LeCun et al. 1989) for CIFAR-10 and a CNN (McMahan et al. 2017) for FEMNIST. We fix the batch size to 20. Clients within a cohort train using the standard FedAvg algorithm utilizing the SGD optimizer with a learning rate of $\eta = 0.002$ and a momentum of 0.9 for CIFAR-10, and $\eta = 0.004$ for FEMNIST. These values are taken from existing works (Hsieh et al. 2020; Dhasade et al. 2023). Clients perform one local epoch in a given round for CIFAR-10 and five local steps for FEMNIST. We consider a network with 200 nodes for CIFAR-10 and take a fixed random subset of 1000 nodes (out of 3550 nodes) for FEMNIST. For CIFAR-10, we experiment with varying degrees of non-IIDness, controlled by α . Specifically, we construct heterogeneous data splits using the Dirichlet distribution, in line with previous work (Hsu, Qi, and Brown 2019; Lin et al. 2020; Gong et al. 2022).

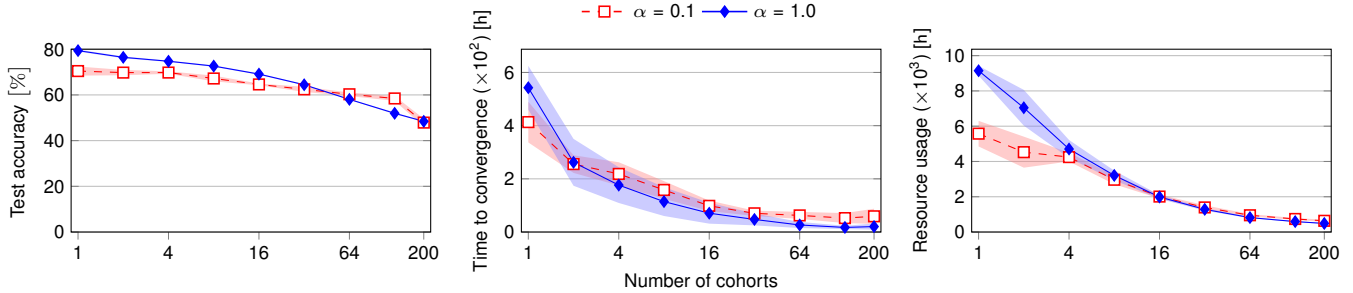


Figure 3: The test accuracy, convergence time and resource usage (in CPU hours) of CIFAR-10, for increasing number of cohorts (n) and different degrees of data distributions (controlled by α). We provide values for $\alpha = 0.3$ in Appendix B.4.

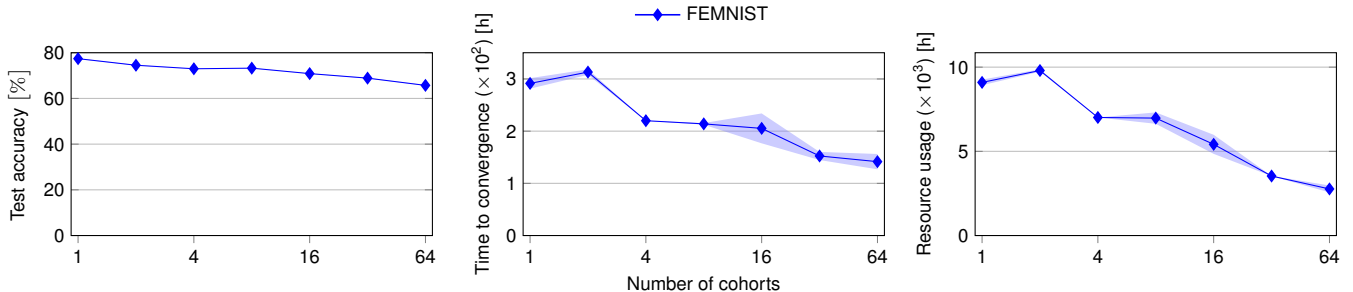


Figure 4: The test accuracy, convergence time and resource usage (in CPU hours) of FEMNIST, for increasing number of cohorts (n).

We experiment with $\alpha = 1$ (IID), $\alpha = 0.3$ (mild non-IID) and $\alpha = 0.1$ (heavily non-IID). FEMNIST follows a natural non-IID partitioning based on the data sample creators.

Distillation. For CIFAR-10, we employ the STL-10 dataset (Coates, Ng, and Lee 2011) for KD, a dataset inspired by CIFAR-10 that has also been utilized in earlier studies (Sattler et al. 2022). This dataset contains 100 000 data samples. For FEMNIST, we use the SVHN dataset, containing 531 131 unlabeled images of house numbers (Sermanet, Chintala, and LeCun 2012). For distillation, we use the Adam optimizer, a learning rate of 0.001, a batch size of 512, and train for 50 epochs.

Validation set. To progress to the second stage of the algorithm, CPFL requires a signal to determine when cohorts have finished training. To achieve this, we have nodes within the cohort compute and report the loss of the global model on a local validation set. This validation set is 10% of the local dataset, and only nodes with at least 10 data samples construct this validation set and report their validation loss. The cohort server collects all validation losses during each round and averages them. A cohort stops model training once the minimum validation loss has not decreased for r rounds. We have conducted various trials, and we found that a value of $r = 50$ for CIFAR-10 and $r = 200$ for FEMNIST achieves a reasonable trade-off between waiting too long and letting cohort models sufficiently converge. We also apply a moving average with a window size of 20 to reduce noise.

Traces. We evaluate CPFL under realistic network environments to provide a closer approximation to real-world

conditions. To this end, we integrate network and compute capacities traces to simulate the hardware performance of nodes (Lai et al. 2022). These traces contain the hardware profile of 131 000 mobile devices and are sourced initially from the AI and MobiPerf benchmarks (Ignatov et al. 2019; Huang et al. 2011). They span a broad spectrum ranging from the network speeds of 130 KB/s to 26 MB/s while the compute speeds vary from 0.9 secs to 11.9 secs to train a mini-batch. We assume that the cohort servers have sufficiently large incoming and outgoing bandwidth capacities that can handle all transfers in a round in parallel.

Finally, we report top-1 test accuracies when evaluating the final model with the test sets. We run each experiment with five different seeds, varying data distribution (for CIFAR-10) and node characteristics, and average all results.

4.2 Resource Savings by CPFL

We first evaluate the test accuracy, time to convergence, and resource usage by CPFL, for CIFAR-10 and FEMNIST under different data distributions (α) and number of cohorts (n). For CIFAR-10, we vary n from 1 to 200; $n = 1$ corresponds to a traditional FL setting, whereas $n = 200$ assigns each node to its own cohort, corresponding to one-shot FedKD as described in Section 2. We remark that one-shot FedKD has only been evaluated with 20 nodes at most, and its performance in larger networks remains unknown.

CIFAR-10. Figure 3 (left plot) shows the test accuracy (in %) of CPFL with the CIFAR-10 dataset across different values of n . To ensure a fair comparison across different val-

ues of n for CIFAR-10, we set the client participation rate to 100% *i.e.*, all nodes in a cohort perform model updates each round. For $n = 1$, an IID data distribution ($\alpha = 1$) achieves the highest accuracy, while a non-IID setting ($\alpha = 0.1$) achieves the lowest accuracy. Figure 3 shows a decreasing trend in test accuracy as n increases. This is because (1) each cohort learns on fewer data as n increases, and (2) KD does not perfectly distill all knowledge. Nonetheless, we notice a marginal drop from 70.4% to 69.8% in test accuracy for $\alpha = 0.1$ when increasing n from 1 (FL) to 4. This same drop is more pronounced for $\alpha = 1$, and we reason this is because KD is less effective in combining knowledge of similar teacher models (see Section 4.5). For $n = 200$ (one-shot FedKD), CPFL achieves 47.9% ($\alpha = 0.1$) to 48.4% ($\alpha = 1$) test accuracy, much lower than what FL obtains.

Figure 3 (middle plot) shows the time to convergence of CPFL for the same evaluated values of n . This is the time between starting model training and training completion by all cohorts. We note a stark decrease in time to convergence as n increases: for $\alpha = 0.1$ and when increasing n from 1 to 4, the time until convergence decreases from 413 hours to 218 hours, a speedup of $1.9\times$ with a minimal loss in test accuracy. This speedup is because cohorts with fewer data samples require less time to converge. Another explanation is that a straggler node, *i.e.*, a node that takes (significantly) longer than other nodes to complete training, does not stall the progression of the entire network but only of its cohort when $n > 1$. In other words, the damage caused by a straggler remains isolated to its cohort. We remark that Figure 3 excludes the time to complete the KD, but we found this to be minimal compared to the overall training time. We provide more details on this in Appendix B.3.

In the non-IID case with $\alpha = 0.1$, CPFL can obtain speedups between $1.6 - 7\times$ as n varies from 2 to 200. These speedups might be particularly beneficial in practical FL settings where one has to execute many runs, *e.g.*, for hyperparameter tuning. For a fixed α and n , we observe a moderate variance in convergence time, which is affected by data distribution and individual resource capabilities.

Figure 3 (right plot) visualizes the resource usage of CPFL regarding CPU hours, representing the total time CPUs spent on training. We observe a reduction in resource usage thanks to the faster convergence of cohort models. In the IID setting ($\alpha = 1$), increasing n from 1 to 4 decreases the required CPU hours from 9145 hours to 4706 hours. The reduction is less pronounced in the non-IID setting ($\alpha = 0.1$), with CPU hours decreasing from 5577 hours to 4249, or $1.3\times$. On the other hand, when increasing n up to 200, a substantial reduction of 8.8 times is achieved for $\alpha = 0.1$, albeit with a trade-off of decreased accuracy. Consequently, in the non-IID case with $\alpha = 0.1$, CPFL demonstrates the potential to reduce resource usage by $1.2 - 8.8\times$ as n varies from 2 to 200.

In a somewhat unexpected observation, we find that non-IID FL ($\alpha = 0.1, n = 1$) converges faster than the IID counterpart ($\alpha = 1, n = 1$) in Figure 3 (middle plot). However, we note that both settings train for a single local epoch in a given round, whereas the IID setting particularly favors more local update steps to exhibit faster convergence. Since

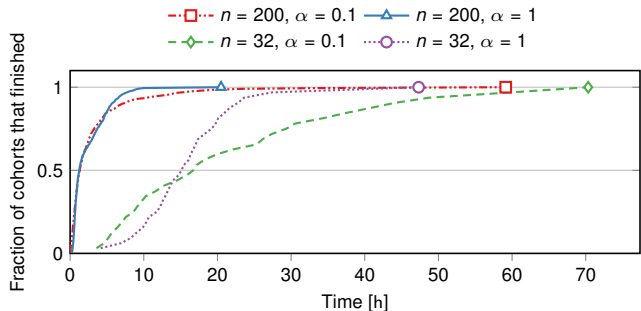


Figure 5: The finish times of individual cohorts, for different numbers of total cohorts and data distributions. We mark the finish time of each group with a symbol.

this is not the case, we observe the above unusual discrepancy. Nevertheless, our experiments show that IID and non-IID cases exhibit a decreasing trend under the same parameter settings. Further, for higher values of n , we observe the anticipated behavior where non-IID setup converges slower than IID. Here, one local epoch likely falls within the desired range of local update steps due to reduced data per cohort, thus exhibiting regular behavior.

We conclude that while FL ($n = 1$) trains more accurate models compared to CPFL, it incurs longer training times and more resource usage. On the other hand, one-shot FedKD ($n = 200$) suffers from accuracy loss but shows great potential to reduce training time and resource usage. CPFL can proficiently navigate these two extremes by controlling the number of cohorts, offering FL practitioners a simple way to tailor FL training sessions according to their requirements.

FEMNIST. Figure 4 (left plot) shows the test accuracy (in %) of CPFL on the FEMNIST dataset across different values of n . Here, we set the client participation rate to 20%. $n = 1$ shows a test accuracy of 77.4%, which gradually decreases to 65.7% for $n = 64$. At the same time, we notice a decreasing trend for the convergence time (middle plot) and resource usage (right plot), although this trend is less pronounced than for CIFAR-10. This is likely because the lower participation rate in each round (20%) reduces the delay that straggler nodes cause as they are selected less frequently compared to network-wide participation. When increasing n from 1 to 4, the convergence time and training resource usage decrease by $1.29\times$ and $1.28\times$, respectively. Nonetheless, Figure 4 shows the benefits of CPFL at a larger scale (1000 nodes) and with partial client participation.

We also observed reductions in communication volume, both for CIFAR-10 and FEMNIST. They follow a similar trend as the reduction in resource usage, and we further comment on this in Appendix B.5. The remaining experiments in this section use the CIFAR-10 dataset as it allows experimentation with different degrees of non-IIDness.

4.3 Training Time of Cohorts

We further analyze the convergence times of cohorts in some of the experiments in Section 4.2. We plot in Figure 5, for

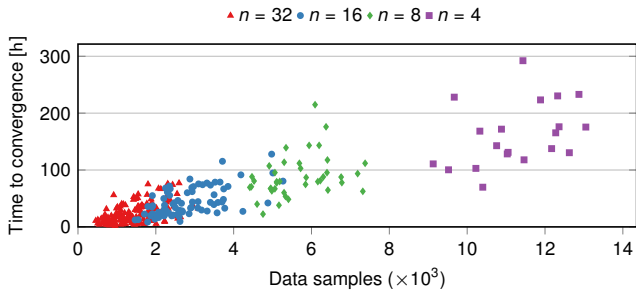


Figure 6: The relation between the number of data samples and the time until convergence within a cohort, for $n = 4, 8, 16$ and 32 , and under a non-IID data distribution ($\alpha = 0.1$).

$n = 32$ and $n = 200$, and $\alpha = 1$ and $\alpha = 0.1$, an ECDF with the fraction of cohorts that completed training as the experiment progressed. These numbers correspond to the experiment described in Section 4.2. In the plot, we annotate the completion of the last cohort in each setting with a marker. Our first observation is that for $n = 200$, 75% of the cohorts converge within less than 5 hours. We do notice some slower cohorts that prolong overall training. Compared to when using $\alpha = 1$, this slowdown is more pronounced for $\alpha = 0.1$, where data distribution is much more skewed. Specifically, for $n = 200$ and $\alpha = 0.1$, the two last cohorts finish training after 34 and 59 hours, respectively. We also notice similar effects for $n = 32$, and we observe a higher variation of training times across cohorts for $n = 32$ and $\alpha = 0.1$, compared to $n = 32$ and $\alpha = 1$. Our results in Figure 5 suggest that FL practitioners can further gain speedups by proceeding to the KD step even when a fraction of cohorts (*e.g.*, 75%) have converged instead of waiting for all cohorts to finish training. This is similar in spirit to how the federated server in traditional FL tolerates partial updates when not all clients complete the expected number of local steps in specified time (Li et al. 2020), albeit at the cost of accuracy.

4.4 Cohort Data Samples and Training Time

CPFL is based on the premise that smaller cohorts *i.e.*, cohorts with fewer clients and consequently with fewer total data samples, converge quicker. To validate this premise, we plot in Figure 6 the relation between the number of total data samples and the time until convergence for every cohort under a non-IID data distribution ($\alpha = 0.1$). We extract results for $n = 4, 8, 16$ and 32 for the experiment runs described in Section 4.2. Figure 6 hints at a positive relation between the number of data samples in a cohort and the time until convergence. Therefore, FL practitioners can manipulate n to increase or decrease the average number of data samples per cohort, subsequently controlling the time required for the cohort to finish training.

4.5 Teacher and Student Accuracies of KD

We now assess the accuracy improvement by KD. We show in Table 1 the average test accuracy of the teacher and student models and the average improvement (Δ), for $\alpha = 0.1$

α	n	Teacher acc.	Student acc.	Δ
0.1	4	65.76 ± 2.63	69.79 ± 0.55	+4.03
	16	48.24 ± 5.86	64.59 ± 0.39	+16.35
	64	27.64 ± 7.38	60.28 ± 0.80	+32.65
	200	17.32 ± 5.67	47.89 ± 1.75	+30.57
1	4	74.44 ± 0.86	74.74 ± 0.30	+0.30
	16	63.37 ± 1.76	69.11 ± 0.34	+5.74
	64	42.44 ± 5.17	58.05 ± 0.24	+15.61
	200	27.00 ± 5.29	48.43 ± 0.27	+21.44

Table 1: The average accuracy of teacher and student models for varying values of α and n , and for the CIFAR-10 dataset. The right-most column shows the improvement in test accuracy by knowledge distillation.

and $\alpha = 1$ across four different values of n . We also report the corresponding standard deviations.

Table 1 shows that increasing n improves the gain in test accuracy induced by KD. This is because, with higher values of n , each cohort trains on proportionately less data, affecting the generalization performance of the teacher models. KD in this case draws a larger *relative* improvement *i.e.*, when unifying many weaker generalizers as opposed to a few good generalizers. We also observe that the gains in accuracy are higher for non-IID settings than IID settings. We suspect this is because in a non-IID setting, KD is more capable of combining models that recognize specialized features compared to IID settings where mostly similar models are produced. This observation also aligns with KD’s original concept as a method to effectively combine knowledge from *specialized* ensembles, shown in (Hinton, Vinyals, and Dean 2015). Finally, the insights from Table 1 explain the more significant drop for the IID case than the non-IID in Figure 3 (left plot).

Experimental conclusion. Our experiments suggest that a reasonable value for the number of cohorts lies between 4 and 16. However, the optimal number of cohorts may vary depending on different datasets and system configurations. Therefore, practitioners should consider these variations when choosing the appropriate configuration of CPFL for their specific use cases.

5 Conclusion

This paper introduced Cohort-Parallel Federated Learning (CPFL), an innovative approach to enhance FL by partitioning the network into several smaller cohorts. The underpinning principle of CPFL is that smaller networks lead to quicker convergence and more efficient resource utilization. By unifying the cohort models with Knowledge Distillation and a cross-domain, unlabeled dataset, we produce a final global model that integrates the contributions from all clients. Our experimental findings confirm that this strategy yields significant advantages in training time and resource utilization without considerably compromising test accuracy. This approach offers practitioners a tangible means to control their FL resource consumption and convergence timelines.

References

- Abdelmoniem, A. M.; Sahu, A. N.; Canini, M.; and Fahmy, S. A. 2023. REFL: Resource-Efficient Federated Learning.
- Ben-David, S.; Blitzer, J.; Crammer, K.; Kulesza, A.; Pereira, F.; and Vaughan, J. W. 2010. A Theory of Learning from Different Domains. *Mach. Learn.*, 79(1–2): 151–175.
- Bistriz, I.; Mann, A.; and Bambos, N. 2020. Distributed distillation for on-device learning. *Advances in Neural Information Processing Systems*, 33: 22593–22604.
- Bonawitz, K.; Eichner, H.; Grieskamp, W.; Huba, D.; Ingerman, A.; Ivanov, V.; Kiddon, C.; Konečný, J.; Mazzocchi, S.; McMahan, B.; et al. 2019. Towards federated learning at scale: System design. *Proceedings of machine learning and systems*, 1: 374–388.
- Briggs, C.; Fan, Z.; and Andras, P. 2020. Federated learning with hierarchical clustering of local updates to improve training on non-IID data. In *2020 International Joint Conference on Neural Networks (IJCNN)*, 1–9.
- Caldas, S.; Duddu, S. M. K.; Wu, P.; Li, T.; Konečný, J.; McMahan, H. B.; Smith, V.; and Talwalkar, A. 2019. Leaf: A benchmark for federated settings. In *2nd Intl. Workshop on Federated Learning for Data Privacy and Confidentiality (FL-NeurIPS)*.
- Charles, Z.; Garrett, Z.; Huo, Z.; Shmulyian, S.; and Smith, V. 2021. On large-cohort training for federated learning. *Advances in neural information processing systems*, 34: 20461–20475.
- Coates, A.; Ng, A.; and Lee, H. 2011. An analysis of single-layer networks in unsupervised feature learning. In *Proceedings of the fourteenth international conference on artificial intelligence and statistics*, 215–223. JMLR Workshop and Conference Proceedings.
- Dhasade, A.; Dresevic, N.; Kermarrec, A.-M.; and Pires, R. 2022. TEE-based decentralized recommender systems: The raw data sharing redemption. In *2022 IEEE International Parallel and Distributed Processing Symposium (IPDPS)*, 447–458. IEEE.
- Dhasade, A.; Kermarrec, A.-M.; Pires, R.; Sharma, R.; and Vujasinovic, M. 2023. Decentralized learning made easy with DecentralizePy. In *Proceedings of the 3rd Workshop on Machine Learning and Systems*, 34–41.
- Duan, M.; Liu, D.; Ji, X.; Wu, Y.; Liang, L.; Chen, X.; Tan, Y.; and Ren, A. 2021. Flexible clustered federated learning for client-level data distribution shift. *IEEE Transactions on Parallel and Distributed Systems*, 33(11): 2661–2674.
- Ghosh, A.; Chung, J.; Yin, D.; and Ramchandran, K. 2020. An efficient framework for clustered federated learning. *Advances in Neural Information Processing Systems*, 33: 19586–19597.
- Gong, X.; Sharma, A.; Karanam, S.; Wu, Z.; Chen, T.; Dormann, D.; and Innanje, A. 2022. Preserving privacy in federated learning with ensemble cross-domain knowledge distillation. In *Proceedings of the AAAI Conference on Artificial Intelligence*, volume 36, 11891–11899.
- He, C.; Annavaram, M.; and Avestimehr, S. 2020. Group knowledge transfer: Federated learning of large cnns at the edge. *Advances in Neural Information Processing Systems*, 33: 14068–14080.
- Hinton, G.; Vinyals, O.; and Dean, J. 2015. Distilling the Knowledge in a Neural Network. In *NIPS Deep Learning and Representation Learning Workshop*.
- Hsieh, K.; Phanishayee, A.; Mutlu, O.; and Gibbons, P. 2020. The non-iid data quagmire of decentralized machine learning. In *International Conference on Machine Learning*, 4387–4398. PMLR.
- Hsu, T.-M. H.; Qi, H.; and Brown, M. 2019. Measuring the effects of non-identical data distribution for federated visual classification. *arXiv preprint arXiv:1909.06335*.
- Huang, J.; Chen, C.; Pei, Y.; Wang, Z.; Qian, Z.; Qian, F.; Tiwana, B.; Xu, Q.; Mao, Z.; Zhang, M.; et al. 2011. Mobiperf: Mobile network measurement system. *Technical Report. University of Michigan and Microsoft Research*.
- Huba, D.; Nguyen, J.; Malik, K.; Zhu, R.; Rabbat, M.; Yousefpour, A.; Wu, C.-J.; Zhan, H.; Ustinov, P.; Srinivas, H.; et al. 2022. Papaya: Practical, private, and scalable federated learning. *Proceedings of Machine Learning and Systems*, 4: 814–832.
- Ignatov, A.; Timofte, R.; Kulik, A.; Yang, S.; Wang, K.; Baum, F.; Wu, M.; Xu, L.; and Van Gool, L. 2019. Ai benchmark: All about deep learning on smartphones in 2019. In *2019 IEEE/CVF International Conference on Computer Vision Workshop (ICCVW)*, 3617–3635. IEEE.
- Krizhevsky, A.; Hinton, G.; et al. 2009. Learning multiple layers of features from tiny images.
- Lai, F.; Dai, Y.; Singapuram, S.; Liu, J.; Zhu, X.; Madhyastha, H.; and Chowdhury, M. 2022. FedScale: Benchmarking model and system performance of federated learning at scale. In *International Conference on Machine Learning*, 11814–11827. PMLR.
- Lai, F.; Zhu, X.; Madhyastha, H. V.; and Chowdhury, M. 2021. Oort: Efficient Federated Learning via Guided Participant Selection. In *15th USENIX Symposium on Operating Systems Design and Implementation (OSDI 21)*, 19–35. USENIX Association. ISBN 978-1-939133-22-9.
- LeCun, Y.; Boser, B.; Denker, J.; Henderson, D.; Howard, R.; Hubbard, W.; and Jackel, L. 1989. Handwritten digit recognition with a back-propagation network. *Advances in neural information processing systems*, 2.
- Li, D.; and Wang, J. 2019. FedMD: Heterogenous Federated Learning via Model Distillation. *NeurIPS Workshop on Federated Learning for Data Privacy and Confidentiality*.
- Li, T.; Sahu, A. K.; Zaheer, M.; Sanjabi, M.; Talwalkar, A.; and Smith, V. 2020. Federated optimization in heterogeneous networks. *Proceedings of Machine learning and systems*, 2: 429–450.
- Lin, T.; Kong, L.; Stich, S. U.; and Jaggi, M. 2020. Ensemble Distillation for Robust Model Fusion in Federated Learning. In Larochelle, H.; Ranzato, M.; Hadsell, R.; Balcan, M.; and Lin, H., eds., *Advances in Neural Information Processing Systems*, volume 33, 2351–2363. Curran Associates, Inc.

- Liu, J.; Lai, F.; Dai, Y.; Akella, A.; Madhyastha, H.; and Chowdhury, M. 2022. Auxo: Heterogeneity-Mitigating Federated Learning via Scalable Client Clustering. arXiv:2210.16656.
- McMahan, B.; Moore, E.; Ramage, D.; Hampson, S.; and y Arcas, B. A. 2017. Communication-efficient learning of deep networks from decentralized data. In *Artificial intelligence and statistics*, 1273–1282. PMLR.
- Sattler, F.; Marban, A.; Rischke, R.; and Samek, W. 2022. CFD: Communication-Efficient Federated Distillation via Soft-Label Quantization and Delta Coding. *IEEE Transactions on Network Science and Engineering*, 9(4): 2025–2038.
- Sattler, F.; Müller, K.-R.; and Samek, W. 2020. Clustered federated learning: Model-agnostic distributed multitask optimization under privacy constraints. *IEEE transactions on neural networks and learning systems*, 32(8): 3710–3722.
- Sermanet, P.; Chintala, S.; and LeCun, Y. 2012. Convolutional neural networks applied to house numbers digit classification. In *Proceedings of the 21st international conference on pattern recognition (ICPR2012)*, 3288–3291. IEEE.
- Zhmoginov, A.; Sandler, M.; Miller, N.; Kristiansen, G.; and Vladymyrov, M. 2023. Decentralized Learning with Multi-Headed Distillation. In *Proceedings of the IEEE/CVF Conference on Computer Vision and Pattern Recognition*, 8053–8063.

A Theoretical Analysis

A.1 Analysis of Section 3.2

We begin by recalling the notations and definitions used throughout the theoretical analysis. We define $\mathcal{H}\Delta\mathcal{H}$ -divergence between a source \mathcal{D}' and target \mathcal{D} distribution as

$$d_{\mathcal{H}\Delta\mathcal{H}}(\mathcal{D}', \mathcal{D}) = 2 \sup_{h, h' \in \mathcal{H}} \left| \mathbb{P}_{x \sim \mathcal{D}'}(h(x) \neq h'(x)) - \mathbb{P}_{x \sim \mathcal{D}}(h(x) \neq h'(x)) \right|$$

Let $h_s = \sum_{i=1}^n p_i h_i$ where $\sum_{i=1}^n p_i = 1$ and $p_i > 0$, denote the hypothesis on the global server and h_i the one on the cohort i . Let \mathcal{D} be any target distribution and \mathcal{D}_i be a mixture of K 's local distribution $\{\mathcal{D}_{i,k}\}_{k=1}^K$, that is, $\mathcal{D}_i = \frac{1}{K} \sum_{k=1}^K \mathcal{D}_{i,k}$. Denote the expected risk of hypothesis h on the distribution \mathcal{D} as $\mathcal{L}_{\mathcal{D}}(h)$. We state the following lemmas.

Lemma 1 (Theorem 3, (Ben-David et al. 2010)). *For any target distribution \mathcal{D} and source distribution \mathcal{D}' . The expected risk of a hypothesis h on the \mathcal{D} is bounded by*

$$\mathcal{L}_{\mathcal{D}}(h) \leq \mathcal{L}_{\mathcal{D}'}(h) + \frac{1}{2} d_{\mathcal{H}\Delta\mathcal{H}}(\mathcal{D}', \mathcal{D}) + \lambda \quad (5)$$

where we note $\lambda = \inf_{h \in \mathcal{H}} \{\mathcal{L}_{\mathcal{D}'}(h) + \mathcal{L}_{\mathcal{D}}(h)\}$

Lemma 2. *Let $\{\mathcal{D}_k\}_{k=1}^K$ be a set of distributions and define $\mathcal{D}' = \frac{1}{K} \sum_{k=1}^K \mathcal{D}_k$. For any distribution \mathcal{D} , the $\mathcal{H}\Delta\mathcal{H}$ -divergence between \mathcal{D}' and \mathcal{D} is bounded by*

$$d_{\mathcal{H}\Delta\mathcal{H}}(\mathcal{D}', \mathcal{D}) \leq \frac{1}{K} \sum_{k=1}^K d_{\mathcal{H}\Delta\mathcal{H}}(\mathcal{D}_k, \mathcal{D}) \quad (6)$$

Proof.

$$\begin{aligned} d_{\mathcal{H}\Delta\mathcal{H}}(\mathcal{D}', \mathcal{D}) &= 2 \sup_{h, h' \in \mathcal{H}} \left| \mathbb{P}_{x \sim \mathcal{D}'}(h(x) \neq h'(x)) - \mathbb{P}_{x \sim \mathcal{D}}(h(x) \neq h'(x)) \right| \\ &= 2 \sup_{h, h' \in \mathcal{H}} \left| \mathbb{P}_{x \sim \frac{1}{K} \sum_{k=1}^K \mathcal{D}_k}(h(x) \neq h'(x)) - \mathbb{P}_{x \sim \mathcal{D}}(h(x) \neq h'(x)) \right| \\ &= 2 \sup_{h, h' \in \mathcal{H}} \left| \frac{1}{K} \sum_{k=1}^K \mathbb{P}_{x \sim \mathcal{D}_k}(h(x) \neq h'(x)) - \mathbb{P}_{x \sim \mathcal{D}}(h(x) \neq h'(x)) \right| \\ &\leq \frac{2}{K} \sum_{k=1}^K \sup_{h, h' \in \mathcal{H}} \left| \mathbb{P}_{x \sim \mathcal{D}_k}(h(x) \neq h'(x)) - \mathbb{P}_{x \sim \mathcal{D}}(h(x) \neq h'(x)) \right| \\ &= \frac{1}{K} \sum_{k=1}^K d_{\mathcal{H}\Delta\mathcal{H}}(\mathcal{D}_k, \mathcal{D}) \end{aligned} \quad (7)$$

□

Theorem 1. *Let \mathcal{H} be a finite hypothesis class and $h_s := \sum_{i=1}^n p_i h_i$, where $p_i > 0$ and $\sum_{i=1}^n p_i = 1$. Suppose that each source dataset has m instances. Then, for any $\delta \in (0, 1)$, with probability at least $1 - \delta$, the expected risk of h_s on the target distribution \mathcal{D} is bounded by:*

$$\mathcal{L}_{\mathcal{D}}(h_s) \leq \sum_{i=1}^n \sum_{k=1}^K \frac{p_i}{K} \mathcal{L}_{\mathcal{D}_{i,k}}(h_i) + \sum_{i=1}^n \sum_{k=1}^K \frac{p_i}{K} \left(\frac{1}{2} d_{\mathcal{H}\Delta\mathcal{H}}(\mathcal{D}_{i,k}, \mathcal{D}) + \lambda_{i,k} \right) + \sqrt{\frac{\log(2nK/\delta)}{2m}} \quad (8)$$

Proof. By the definition of h_s and Jensen inequality, we have

$$\mathcal{L}_{\mathcal{D}}(h_s) := \mathcal{L}_{\mathcal{D}} \left(\sum_{i=1}^n p_i h_i \right) \leq \sum_{i=1}^n p_i \mathcal{L}_{\mathcal{D}}(h_i) \quad (9)$$

Using Lemma 1, the expected risk of h_i on \mathcal{D} is bounded by

$$\mathcal{L}_{\mathcal{D}}(h_i) \leq \mathcal{L}_{\mathcal{D}_i}(h_i) + \frac{1}{2} d_{\mathcal{H}\Delta\mathcal{H}}(\mathcal{D}_i, \mathcal{D}) + \lambda_i \quad (10)$$

where we note $\lambda_i = \inf_{h \in \mathcal{H}} \mathcal{L}_{\mathcal{D}}(h) + \mathcal{L}_{\mathcal{D}_i}(h)$. Let $\mathcal{D}_i = \frac{1}{K} \sum_{k=1}^K \mathcal{D}_{i,k}$ a mixture of distributions in cohort i , we have then

$$\begin{aligned}
\mathcal{L}_{\mathcal{D}}(h_i) &\leq \mathcal{L}_{\mathcal{D}_i}(h_i) + \frac{1}{2} d_{\mathcal{H}\Delta\mathcal{H}}(\mathcal{D}_i, \mathcal{D}) + \lambda_i \\
&\leq \mathcal{L}_{\mathcal{D}_i}(h_i) + \frac{1}{2K} \sum_{k=1}^K d_{\mathcal{H}\Delta\mathcal{H}}(\mathcal{D}_{i,k}, \mathcal{D}) + \lambda_i \\
&\leq \frac{1}{K} \sum_{k=1}^K \mathcal{L}_{\mathcal{D}_{i,k}}(h_i) + \frac{1}{2K} \sum_{k=1}^K d_{\mathcal{H}\Delta\mathcal{H}}(\mathcal{D}_{i,k}, \mathcal{D}) + \lambda_i \\
&\leq \frac{1}{K} \sum_{k=1}^K \mathcal{L}_{\mathcal{D}_{i,k}}(h_i) + \frac{1}{2K} \sum_{k=1}^K d_{\mathcal{H}\Delta\mathcal{H}}(\mathcal{D}_{i,k}, \mathcal{D}) + \frac{1}{K} \sum_{k=1}^K \lambda_{i,k}
\end{aligned} \tag{11}$$

where the second inequality is application of Lemma 2. The third one follows the fact that $\mathcal{D}_i = \frac{1}{K} \sum_{k=1}^K \mathcal{D}_{i,k}$. The last inequality follows the same fact and application of triangle and Jensen's inequality on λ_i . Using Hoeffding's inequality, with probability $1 - \frac{\delta}{nK}$, the risk of hypothesis h_i on the source distribution $\mathcal{D}_{i,k}$ is upper bounded by

$$\mathcal{L}_{\mathcal{D}_{i,k}}(h_i) \leq \mathcal{L}_{\hat{\mathcal{D}}_{i,k}}(h_i) + \sqrt{\frac{\log(2nK/\delta)}{2m}} \tag{12}$$

where $\mathcal{L}_{\hat{\mathcal{D}}_{i,k}}(h_i)$ is the risk of h_i on the empirical distribution $\hat{\mathcal{D}}_{i,k}$. Combining Equations (9), (11) and (12) and using the same analysis as in (Lin et al. 2020). With probability at least $1 - \delta$ over nK sources of m samples, we have :

$$\begin{aligned}
\mathcal{L}_{\mathcal{D}}(h_s) &\leq \sum_{i=1}^n \sum_{k=1}^K \frac{p_i}{K} \mathcal{L}_{\mathcal{D}_{i,k}}(h_i) + \sum_{i=1}^n \sum_{k=1}^K \frac{p_i}{2K} d_{\mathcal{H}\Delta\mathcal{H}}(\mathcal{D}_{i,k}, \mathcal{D}) + \sum_{i=1}^n \sum_{k=1}^K \frac{p_i}{K} \lambda_{i,k} \\
&\leq \sum_{i=1}^n \sum_{k=1}^K \frac{p_i}{K} \mathcal{L}_{\hat{\mathcal{D}}_{i,k}}(h_i) + \sum_{i=1}^n \sum_{k=1}^K \frac{p_i}{K} \sqrt{\frac{\log(2nK/\delta)}{2m}} + \sum_{i=1}^n \sum_{k=1}^K \frac{p_i}{2K} d_{\mathcal{H}\Delta\mathcal{H}}(\mathcal{D}_{i,k}, \mathcal{D}) + \sum_{i=1}^n \sum_{k=1}^K \frac{p_i}{K} \lambda_{i,k} \\
&\leq \sum_{i=1}^n \sum_{k=1}^K \frac{p_i}{K} \mathcal{L}_{\hat{\mathcal{D}}_{i,k}}(h_i) + \sum_{i=1}^n \sum_{k=1}^K \frac{p_i}{K} \left(\frac{1}{2} d_{\mathcal{H}\Delta\mathcal{H}}(\mathcal{D}_{i,k}, \mathcal{D}) + \lambda_{i,k} \right) + \sqrt{\frac{\log(2nK/\delta)}{2m}}
\end{aligned} \tag{13}$$

□

B Additional Notes on Experimental Evaluation

B.1 Compute Infrastructure and Implementation

We run all experiments on machines in our compute cluster. Each machine is equipped with dual 24-core AMD EPYC-2 CPU, 128 GB of memory, a NVIDIA RTX A4000 GPU, and is running CentOS 8. For reproducibility and in line with related work in the domain, we simulate the passing of time in our experiments (Lai et al. 2022, 2021; Abdelmoniem et al. 2023). We achieve this by customizing the default event loop provided by the `asyncio` library and processing events without delay. This requires minimal changes to the code, and therefore our implementation can be made suitable for usage in a production environment with trivial changes.

B.2 Motivational Plot (Figure 2)

Figure 2, showing the evolution of validation loss and motivating the approach behind CPFL, has been generated from the CIFAR-10 experiments described in Section 4.2. These plots correspond to the validation loss for each of the four cohorts, in a setting with $n = 4$ and when using 90 as seed, for $\alpha = 1$ and $\alpha = 0.3$.

In Figure 2, we chose to highlight the results of a single run rather than averaging across multiple runs. The rationale behind this decision stems from the fact that when averaging, the stopping criterion which applies to individual runs does not hold any meaningful interpretation for the averaged result. This means that an average might misrepresent the number of rounds required for convergence or even the validity of the stopping criterion itself. By focusing on a single run, we ensure the integrity and applicability of our stopping criterion, providing a clearer and more direct interpretation of our results. We have manually verified that our conclusion also hold true for different seeds and number of cohorts.

B.3 Knowledge Distillation

Figure 3 excludes the time it takes for the KD process to complete. For CIFAR-10, we noticed that KD takes between 50 minutes (for $n = 2$) and 305 minutes (for $n = 200$) to complete. This time frame represents a small fraction of the time and resources required for model training by cohorts. Regarding FEMNIST, the KD process takes between 59 minutes (for $n = 2$) and 16.8 hours (for $n = 64$). In the case of FEMNIST, the majority of time is spent on generating inferences from the teacher models. We propose two methods to expedite this process. First, one can parallelize this process by generating logits from distinct teacher models simultaneously. Second, one can increase the inference batch size, although at the cost of additional memory usage.

B.4 CIFAR-10 Results with $\alpha = 0.3$

We show in Figure 7 the test accuracy, convergence time and resource usage (CPU hours) of the CIFAR-10 dataset. Compared to Figure 3, this plot includes the $\alpha = 0.3$ setting that we omitted from Figure 3 for presentation clarity.

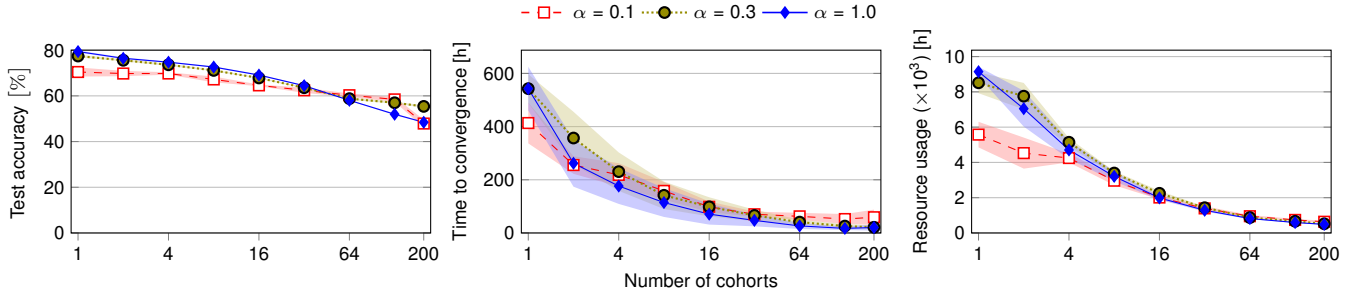


Figure 7: The test accuracy, convergence time and resource usage (in CPU hours) of CIFAR-10, for increasing number of cohorts (c) and different degrees of data distributions (controlled by α).

B.5 Savings in Communication Volume by CPFL

Besides savings in training time and CPU resource usage (see Figure 3 and 4), CPFL also provides savings in communication volume. Figure 8 shows the communication volume required by CPFL, for the CIFAR-10 and FEMNIST dataset, and for different number of cohorts (n). The trend in communication volume as n increases is comparable to the trend in time to convergence and resource usage shown in figure 3 and Figure 4. For CIFAR-10 with $n = 200$, since each node will perform standalone training of its model, we remark that the only communication volume incurred is when sending the trained cohort model to the global server.

For the same value of n , we notice that FEMNIST incurs significantly more communication volume compared to CIFAR-10. This is because the model size of FEMNIST in serialized form is significantly larger than that of CIFAR-10, namely 6.7 MB for FEMNIST compared to 346 KB for CIFAR-10. Additionally, FEMNIST also requires many more rounds to converge than CIFAR-10 due to the large overall network size (1000 nodes) and the challenging nature of the 62-class classification task. As a result, this leads to escalated communication costs.

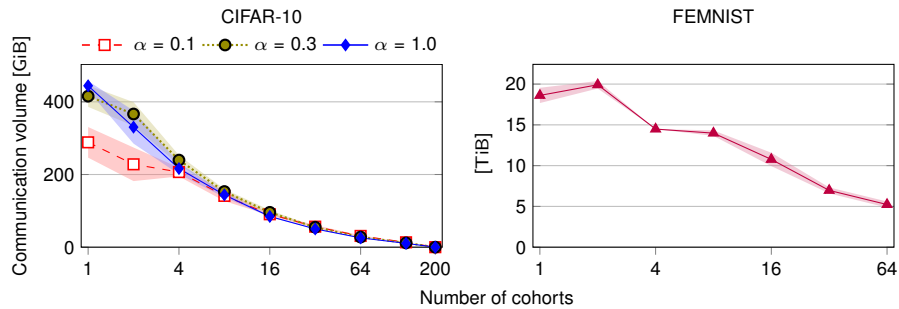


Figure 8: The communication volume required by CPFL for convergence, for CIFAR-10 and FEMNIST, and for different number of cohorts (n). For CIFAR-10 we also show the communication volume for different values of α .